

Article

On the Successiveness of the Two Extreme Cold Events in China during the 2020/21 Winter According to Cold Air Trajectories

Leying Zhang¹, Shuxiu Hou¹ and Zuowei Xie^{2,*} 

¹ Collaborative Innovation Center of Sustainable Forestry in Southern China of Jiangsu Province, College of Biology and Environment, Nanjing Forestry University, Nanjing 210037, China

² International Center for Climate and Environment Sciences, Institute of Atmospheric Physics, Chinese Academy of Sciences, Beijing 100029, China

* Correspondence: xiezuowei@mail.iap.ac.cn

Abstract: Two extreme cold air events successively hit China during 28–31 December 2020 (the late 2020 event) and during 6–8 January 2021 (the early 2021 event), which caused great losses. These two events have received extensive attention in relation to synoptic weather systems and remote forcing. Although it has been noted that a near-surface cool condition can greatly impact tropospheric circulation, its role in the successiveness of two such extreme cold waves remains unclear. This study focused on cold air pathways from the Lagrangian perspective, and explored the potential influence of cold air over the key region in terms of connecting the two cold events using a piecewise potential vorticity inversion. With the obtained results, three cold air sources with three corresponding air routes were identified in the two cold events. The northern pathway dominated the late 2020 event, in which the cold air intruded from the eastern Laptev Sea and moved southward to China. In contrast, the early 2021 event was mainly associated with the northwestern pathway in which the cold air came from the Ural Mountains and moved clockwise. Notably, cold air traveling along the western route from western Lake Balkhash arrived at the north of the Tianshan Mountains earlier and amplified the positive height anomaly in situ. Moreover, such an enhanced positive height anomaly moved the direction of the cold air from the northern and northwestern routes southward and thus played a key role in the successiveness of the two extreme cold events.

Keywords: extreme event; cold air pathway; successive; surface cold air; piecewise potential vorticity inversion



Citation: Zhang, L.; Hou, S.; Xie, Z. On the Successiveness of the Two Extreme Cold Events in China during the 2020/21 Winter According to Cold Air Trajectories. *Atmosphere* **2022**, *13*, 1915. <https://doi.org/10.3390/atmos13111915>

Academic Editors: Shuangyan Yang and Yanjun Qi

Received: 19 October 2022

Accepted: 8 November 2022

Published: 17 November 2022

Publisher's Note: MDPI stays neutral with regard to jurisdictional claims in published maps and institutional affiliations.



Copyright: © 2022 by the authors. Licensee MDPI, Basel, Switzerland. This article is an open access article distributed under the terms and conditions of the Creative Commons Attribution (CC BY) license (<https://creativecommons.org/licenses/by/4.0/>).

1. Introduction

China was hit by two successive extreme cold air events during 28–31 December 2020 (called “the late 2020 event” for brevity) and during 6–8 January 2021 (“the early 2021 event”). These two rarely occurring events showed unique features in their intensity, impact area, and economic damage, which were ranked in the third and second percentiles among all winters since 1979 [1]. In the late 2020 event, an 8°C (12°C) temperature drop swept across more than 4 (1.75) million square kilometers, indicating that almost half of the Chinese mainland reached the cold wave level, while 2.5 (0.4) million square kilometers were affected in the early 2021 event [2]. More severely, the early 2021 event occurred on the heels of the late 2020 event, with continuous cooling. As a result, the temperature of the early 2021 event was lower and more severe despite its smaller temperature drop. These two successive extreme events occurring in such a short period of time have invited much attention, and their causative factors have been extensively explored from synoptic weather systems to remote forcing [1–6].

The key synoptic weather system in both events was recognized as a kind of “anti-clockwise turning of a transverse trough” accompanying a blocking ridge (or blocking high) from the Kara Sea to Lake Baikal in the late 2020 event and the east of the Ural Mountains

in the early 2021 event, respectively [2,7]. This blocking ridge dominated these two events without the usual breakdown or “discontinuous westward shift”, resulting in the maintenance and enhancement of the northerlies in front of the ridge and leading to an increase in baroclinicity in situ [7]. On the other side, the ridge also benefited the development and anticlockwise turning of a downstream trough via Rossby energy dispersion [2]. These enhanced the Siberian High and its southward extending, triggering the cold events.

In the stratosphere, a polar vortex trough (or a major sudden stratospheric warming) deepened from Scandinavia to Western Europe in the late 2020 event with a positive potential vorticity (PV) anomaly [1]. The positive PV anomaly intensified the tropospheric low anomaly underneath [8], facilitating the wave train propagation from Scandinavia to East Asia and amplifying meridional circulation, thereby causing a cold air outbreak in East Asia. Then, the stratospheric polar vortex trough split into two parts in the early 2021 event. One center over Northeast Asia deepened the East Asian trough, driving the cold polar air mass to spread southward. Yu et al. [6] also underscored the stratospheric downward influence from the isentropic mass circulation perspective. The poleward warm branch of the meridional mass circulation was strengthened in the stratosphere, which enhanced the equatorward cold branch in the troposphere, inducing the southward expansion of polar surface high anomalies, which are conducive to cold events. Furthermore, the Arctic Sea ice loss in autumn, the warm North Atlantic blob, and cold sea surface temperatures in the central-eastern Pacific could have benefited the stratospheric polar vortex trough and strengthened tropospheric blockings, which thus favor cold events [1,4,9,10].

Aside from the impact of upper stratosphere circulation and remote forcing, the surface cold anomaly has a nonnegligible influence on the tropospheric circulation. Bretherton [11] proposed that the surface cold anomaly acts as an anticyclonic PV anomaly that influences aloft air circulation by modifying the static stability. The surface cold anomaly increases baroclinic growth, where the mid- and upper-tropospheric blocking circulation and the near-surface high mutually intensify each other, resulting in cold events [12–15]. Given that surface cold mimics the negative PV anomaly (i.e., anticyclonic circulation), it is of interest to investigate its role in cold-air outbreaks. However, this has not yet been analyzed. Cold air paths have always been crucial for the prediction of cold events [16–18]. It is widely recognized that central Siberia (70° E– 90° E, 43° N– 65° N) is the key region for cold events in the Chinese mainland, where the cold air accumulates from different sources, becomes enhanced, and then invades the Chinese mainland southward [19,20]. Bueh et al. [2] identified the northwestern path from the northern Ural Mountains and the northern path from the north of Lake Baikal in terms of the 24h surface temperature drop. Although these two cold air extremes have been attributed to the persistent aloft blocking high, whether there is a linkage between these two cold events remains unknown.

By adopting a perspective based on prior findings, this study tries to answer the following two questions to make a new contribution to our understanding of the successiveness of the two extreme cold events. First, what are the cold air routes and the key region in these two successive cold events? Second, what physical processes occur in terms of cold air over the key region in the successiveness of the two events? Thus, we used a trajectory-analysis method based on the Lagrangian framework to track the cold air paths. The trajectories were classified using the *K*-means method to identify the major cold air paths and key regions. Then, a piecewise quasi-geostrophic PV inversion was applied to the thermal anomaly over the key region to investigate its connecting impacts on the cold air outburst. We describe our data and methods in Section 2. Section 3 presents the cold air trajectories for the two events. Section 4 presents the evaluation of the role of cold air over the key region in the successive extreme cold events. The final section provides the conclusion and discussion.

2. Materials and Methods

2.1. Data

In this study, we used daily atmospheric data from the fifth-generation European Center for Medium-Range Weather Forecasts' atmospheric reanalysis of the global climate (ERA5; [21]). The variables used here were the temperature at 2 m above the surface (T2m), sea level pressure, three-dimensional air temperature, geopotential height, and winds. These daily mean fields were derived from the hourly data on a $1.0^\circ \times 1.0^\circ$ longitude–latitude grid. The pressure levels were equally spaced every 50 hPa between 1000 and 100 hPa. To trace the trajectories of the cold air masses, we also used the surface pressure at 6-hour intervals, three-dimensional winds, and air temperature at 68 model levels near the surface from the ERA5 reanalysis data on a $0.25^\circ \times 0.25^\circ$ grid over the region ($10^\circ \text{ N}–90^\circ \text{ N}$, $30^\circ \text{ W}–160^\circ \text{ E}$).

2.2. Cold Air Trajectory Tracing

We used the LAGRANTO analysis tool version 2.0 [22] to calculate the backward trajectories for the two events. LAGRANTO was driven by three-dimensional 6-hour-interval wind fields, which began at 1800 UTC on the final day of each event. The horizontal start points in LAGRANTO were equidistantly distributed with 90 km spacing (corresponding to $\sim 1^\circ$ grid) over the region ($20^\circ \text{ N}–50^\circ \text{ N}$, $95^\circ \text{ E}–135^\circ \text{ E}$). Only the extreme cold points, whose temperature drops were below the average temperature drop during each cold event, were selected for tracking. The end points were the corresponding starting grid points 7 days prior to the events (i.e., 25 December for the late 2020 event and 2 January for the early 2021 event). The routes between the start and end points were considered as the trajectories for each event. Following Bieli et al. [23], the trajectories were initiated at three pressure levels (10, 30, and 50 hPa) above the surface to verify the cold air pathway. In addition, the longitude, latitude, temperature, pressure, and potential temperature were evaluated at every time point.

2.3. Clustering Cold Air Trajectories with the K-Means Method

K-means clustering was used to classify the cold air trajectories. This is an unsupervised learning algorithm that classifies a large data set into a small number of clusters on the basis of the smallest mean distance between each pair of samples [24,25]. To determine the optimum number of air trajectory clusters, we repeated the K-means procedure with a prespecified number from 2 to 10 and computed the silhouette coefficient (S) of each cluster and the averaged silhouette coefficient of all the samples in this clustering (\bar{S}).

$$s(i) = \frac{b(i) - a(i)}{\max\{a(i), b(i)\}}, \quad (1)$$

$$S = \frac{1}{N} \sum_{i=1}^N s(i), \quad (2)$$

$$\bar{S} = \frac{1}{M} \sum_{i=1}^M s(i), \quad (3)$$

where $s(i)$ is the silhouette coefficient of each sample i , and $a(i)$ is the mean distance between the sample i and the others in the same cluster. If only one sample exists in the cluster, $s(i) = 0$. $b(i)$ is the minimum mean distance between the sample i and the samples in other clusters. S is the silhouette coefficient of each cluster and N is the sample number of the corresponding cluster. M is the sample number of the data set. \bar{S} is the averaged silhouette coefficient of all the M samples. \bar{S} ranges from -1 to $+1$. If \bar{S} approaches 0, it represents overlapping clusters with samples very close to the decision boundary of the neighboring clusters. A negative \bar{S} $\{-1, 0\}$ indicates that the samples might have been assigned to the wrong clusters. If \bar{S} is 1, the cluster is dense and well-separated from the other clusters [26,27]. In addition, S in one subcluster larger than \bar{S} suggests that this subcluster is appropriate, and vice versa.

2.4. Piecewise Quasi-Geostrophic PV Inversion

The piecewise quasi-geostrophic PV inversion can distinguish the relative contribution of each PV anomaly and the boundary thermal anomaly to one certain circulation. We used this to investigate the contribution of a surface cold anomaly to the near-surface high [12,28]. The quasi-geostrophic PV anomaly is defined as:

$$q' = \frac{1}{fa^2 \cos^2 \varphi} \frac{\partial^2 \Phi'}{\partial \lambda^2} + \frac{1}{a^2 \cos \varphi} \frac{\partial}{\partial \varphi} \left(\frac{\cos \varphi}{f} \frac{\partial \Phi'}{\partial \varphi} \right) + f \frac{\partial}{\partial p} \left(\frac{1}{\sigma_p} \frac{\partial \Phi'}{\partial p} \right) = \mathcal{L}(\Phi'), \quad (4)$$

where Φ' is the geopotential height anomaly relative to its climatological mean over 1979–2021. σ_p is atmospheric static stability. φ , λ , a , f and p are latitude, longitude, earth radius, Coriolis force parameter and pressure, respectively. The PV anomaly is the Laplace operator (\mathcal{L}) of the geopotential height anomaly, and the geopotential height anomaly can be inverted using suitable boundary conditions [8]. Consistent with Nielsen-Gammon and Lefevre [28], the lower boundary condition is conventionally specified using the boundary potential temperature anomaly θ' :

$$\frac{\partial \Phi'}{\partial p} = -\frac{R}{p} \left(\frac{p}{p_0} \right)^{R/c_p} \theta', \quad (5)$$

where R is the gas constant for dry air, c_p is the specific heat of dry air at the constant pressure and p_0 is 1000 hPa. Therefore, the boundary conditions incorporate the influence of a surface air temperature anomaly on the tropospheric circulations.

3. Cold Air Trajectories in the Two Events

Figure 1 shows the minimum T2m and the average T2m drop during the two events, which are consistent with the results from meteorological observation stations [1,2]. The -20°C of the minimum T2m for both of the extreme cold waves almost reached the Hetao Plains, breaking many local records for the lowest recorded temperatures [2]. The -10°C and -5°C isotherms significantly extended southward due to successive cold air accumulation in the early 2021 event. Accordingly, the average T2m drop center also shifted from central Inner Mongolia and eastern China in the late 2020 event southward to the Hetao Plains and southern China in the early 2021 event.

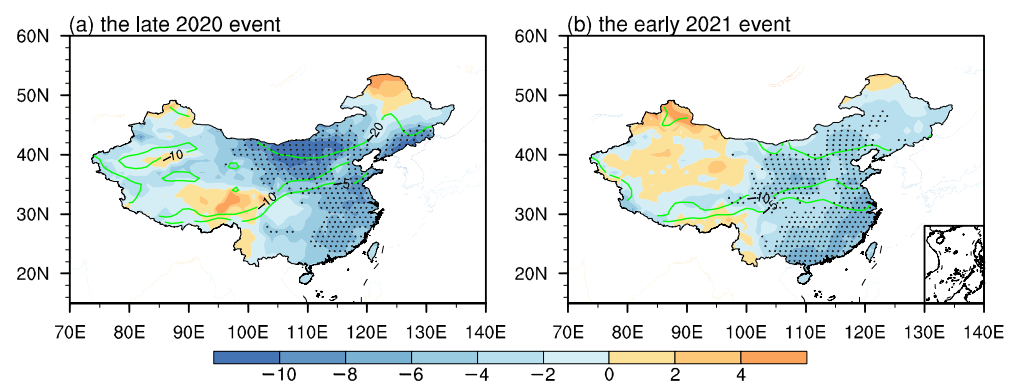


Figure 1. Average temperature drop (shading, unit: $^\circ\text{C}$) in the late 2020 event and the early 2021 event. The average temperature drop is the T2m averaged during the event relative to the T2m on the day before the beginning of the event. The green contours are the minimum T2m on 29 December 2020 and 7 January 2021, respectively. Black dots indicate the starting points for the air trajectory tracking.

To focus on the extreme cold air masses, only the grids in LAGRANTO with a temperature drop larger than the average temperature drop over eastern China (20°N – 50°N , 95°E – 125°E) were selected as the starting tracking points, which was 4.9°C (3.4°C) in the late 2020 event (the early 2021 event). As a result, 298 points were selected in the late

2020 event and 381 points in the early 2021 event, which mainly covered the cold centers (Figure 1). Figure 2 provides the averaged spatial density distribution of the air trajectory tracked using LAGRANTO. Three air sources appeared in the two events. For the late 2020 event, the northern cold air source was over the eastern Laptev Sea, and the northwestern source and the western source were over the west of the Ural Mountains and over the west of Lake Balkhash and the Tianshan Mountains, respectively (Figure 2a). The cold air masses from the eastern Laptev Sea discretely shifted southward around Lake Baikal with a span of 20 degrees of longitude, while those from the northwestern source and the western source merged over the east of Lake Balkhash and moved along the north of the Qinghai–Tibet Plateau (Figure 2a). The northern cold air source in the early 2021 event was the eastern Laptev Sea, similar to the late 2020 event but located southward (Figure 2b). The northwestern source was the Ural Mountains, and the western source was the northern Tianshan Mountains; both are about 20° east of the corresponding sources in the late 2020 event. The cold air from the Ural Mountains dominated the early 2021 event, merged with that from the eastern Laptev Sea over the west of Lake Baikal, and intensively moved southeastward to the middle reaches of the Yangtze River (Figure 2b). The air trajectory densities tracked from 10 and 30 hPa above the surface bore a high similarity with those at 50 hPa (Figure 2), suggesting that they were not sensitive to the starting levels. Therefore, we analyzed the backward air trajectories from 50 hPa, as described in the following paragraphs.

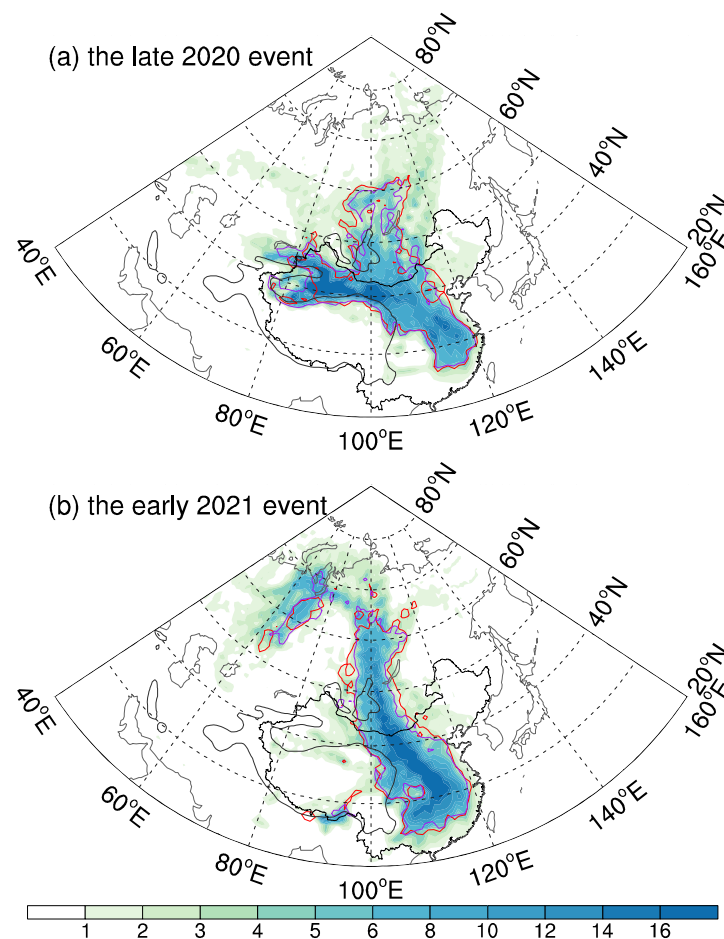


Figure 2. Averaged trajectory density (number of trajectory points associated with each grid point) during the 7 days prior to the final day of the late 2020 event and the early 2021 event starting at 50 hPa. The red and purple lines represent the 5 density contours starting at 10 and 30 hPa, respectively. The black contours indicate the 2000 m terrain height.

To corroborate the difference between the cold air paths in the two events, we further used the *K*-means method to classify the backward air trajectories in LAGRANTO. As cold air moves along the isentropic surface in adiabatic and frictionless flows, the normalized latitude and longitude together with the potential temperature were selected as the classified variables. Figure 3a shows the averaged silhouette coefficient (\bar{S}) of each cluster, which reached maximum when the air trajectories were grouped into three clusters. Moreover, the silhouette coefficients of three subclusters (*S*) all exceeded the averaged silhouette coefficient (Figure 3b), suggesting that three is the optimum number of air trajectory clusters.

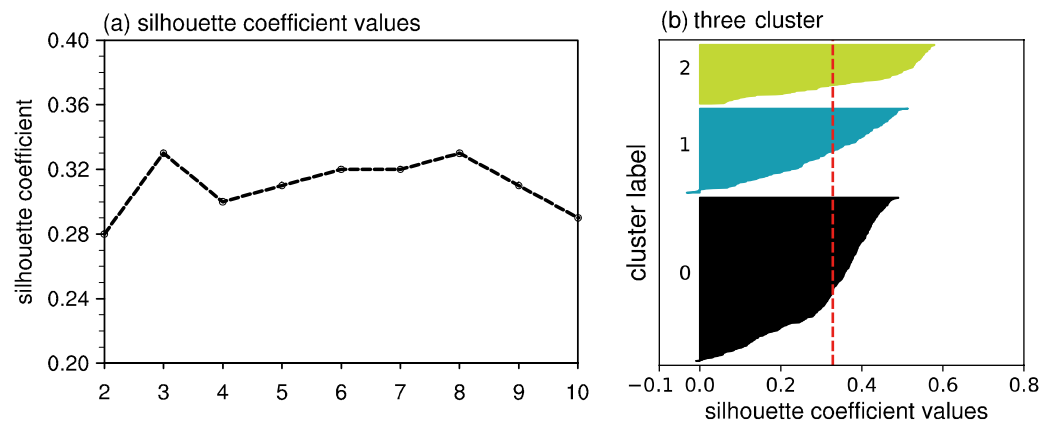


Figure 3. (a) Silhouette coefficients in clusters 2–10 and (b) Silhouette coefficients (red dashed line) and each sample number in three cluster.

Figure 4 shows the air trajectories for the three clusters. Cluster 1, with an averaged 275 K potential temperature, accounted for 55.4% of the total air trajectories (Figure 4a,d,g). For the late 2020 event, the cold air masses originated from the eastern Laptev Sea and western Lake Baikal, the latter may be the pioneering branch of the former from the air trajectories (Figure 4d). The cold air in cluster 1 headed southward and hit North and East China. The cold air from the eastern Laptev Sea and northern Ural Mountains merged over the west of Lake Baikal and intruded southeastern China for the early 2021 event (Figure 4g). The cold air path that came from the northern source (the eastern Laptev Sea) and headed southward is named “the northern route”. Cluster 2 accounted for 26.4% of the total air trajectories, which mostly came from the late 2020 event, with an averaged 285 K potential temperature (Figure 4b,e,h). The cold air of the late 2020 event from the west of the Ural Mountains moved clockwise, while that from the west of Lake Balkhash and the Tianshan Mountains moved eastward to central Inner Mongolia, named “the northwestern route” and “the western route”, respectively (Figure 4e). Similarly, 11.5% of the cold air masses moved along the western route and further invaded the eastern Qinghai-Tibet Plateau in the early 2021 event (Figure 4h). Cluster 3 accounted for 18.3%, with an averaged 275 K potential temperature, and mostly came from the early 2021 event along the northwestern route (Figure 4c,f,i). The cold air masses originated from the Ural Mountains, moved clockwise, and invaded north China (Figure 4i), further eastward than the late 2020 event (Figure 4e,i).

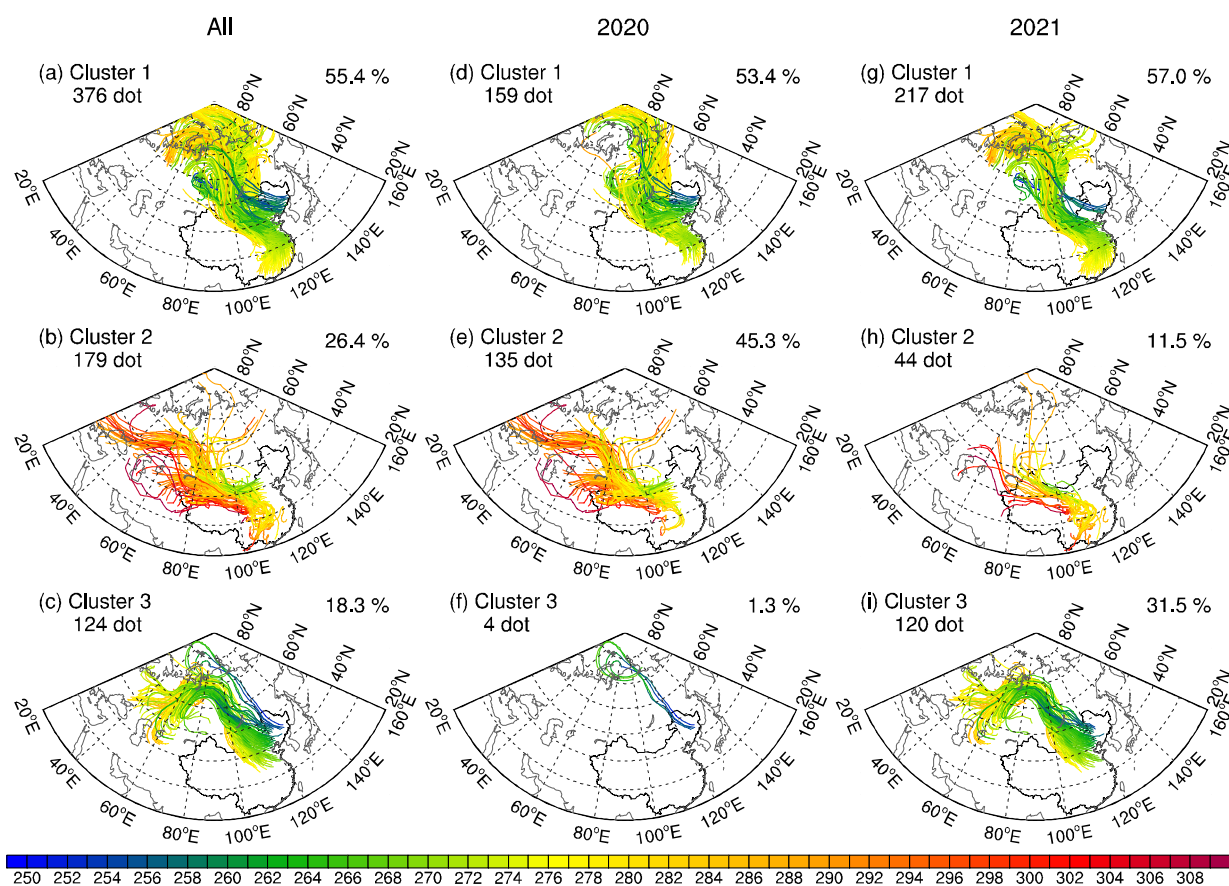


Figure 4. Cold air trajectories (line) and the corresponding potential temperatures (shading, unit: K) during 7 days before the final day of the two events for (a,d,g) cluster 1, (b,e,h) cluster 2, and (c,f,i) cluster 3. Trajectories in (a–c) are all the trajectories in two events, while those in (d–f) and (g–i) are in the 2020 and 2021 events, respectively.

Figure 5 shows the circulation anomalies and the daily air mass locations during the two cold events. The cold air arriving in North and East China travelled along the northern route, while that invading central Inner Mongolia travelled along the northwestern and western routes in the late 2020 event. The cold air masses from the eastern Laptev Sea moved along the northerlies east of the high over the Kara Sea (the Kara Sea High) and accumulated around the transversal trough east of the Ural Mountains before 25 December 2020 (Figure 5a). On 27 December 2020 (Figure 5b), the Kara Sea High shifted southward and helped the transversal trough develop into a meridional trough aided by low-frequency Rossby energy dispersion [2]. The increased northerlies between the ridge and the trough transported the cold air masses southward. Meanwhile, a ridge over the west of the Ural Mountains developed on 25 December and shifted eastward to the Ural Mountains on 27 December (Figure 5a,b). Accordingly, the cold air masses from the west of the Ural Mountains moved along the ridge, featuring a clockwise path (Figure 5a,b). In addition, some cold air masses over the west of Lake Balkhash and the Tianshan Mountains moved along the local westerlies to the north of the Tianshan Mountains on 27 December (Figure 5b). On 29 December 2020, the ridge over the Ural Mountains was incorporated into the Kara Sea High, and the downstream trough was significantly enhanced (Figure 5c). The cold air from the eastern Laptev Sea headed southward to North and East China along the strong northerlies and northwesterlies between the ridge and the trough from 29 December to 31 December (Figure 5c,d). The cold air in the northwestern route merged with that in the western route over eastern Inner Mongolia on 29 December (Figure 5c), and moved eastward to central Inner Mongolia on 31 December (Figure 5d).

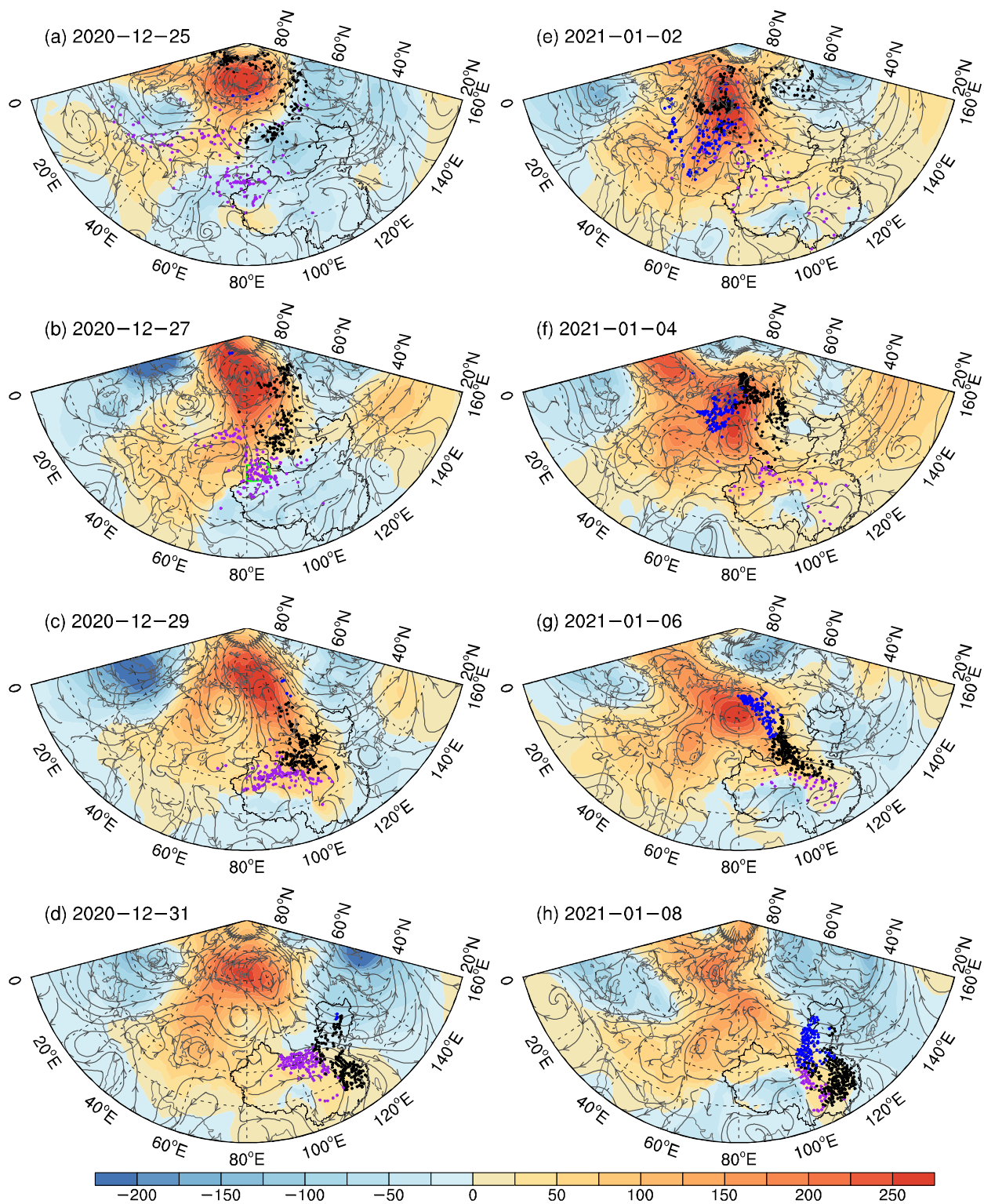


Figure 5. The geopotential height anomaly (shadings, unit: gpm) and wind stream (arrows, units: m/s) at 850 hPa on (a) 25 December 2020, (b) 27 December 2020, (c) 29 December 2020, (d) 31 December 2020, (e) 2 January 2021, (f) 4 January 2021, (g) 6 January 2021, and (h) 8 January 2021. The dots indicate the location of air mass in the corresponding day. The black, purple and blue dots represent the air masses in cluster 1, 2 and 3, respectively. The green box in (b) is the key region over (42° N–47° N, 80° E–90° E).

In the early 2021 event, the cold air along the western, northern, and northwestern routes hit the eastern Qinghai–Tibet Plateau, South China, and North China, respectively (Figure 5e–h). The cold air masses in cluster 1 and cluster 3 were almost all along the blocking ridge over the Ural Mountains on 2 January 2021, as well as over the southern part of Lake Laptev in cluster 1 (Figure 5e). The ridge shifted southward with the development of the East Asian trough during 4–6 January and weakened on 8 January (Figure 5f–h). Accordingly, these cold air masses in cluster 1 and cluster 3 were transported by the northerlies in front of the ridge and sequentially entered South and North China. In addition, the cold air masses in cluster 2 along the western route were in line with those observed in the late 2020 event, which arrived at the north of the Tianshan Mountains earlier than those in the northern and the northwestern routes (Figure 5e,f). Note that the air masses from the Ural Mountains moved clockwise and dominated the early 2021 event according to the air trajectory density (Figure 2b). However, cluster 1 accounted for 57.0% of the air routes (Figure 4g). As can be seen from the locations and movement paths, the air masses along the blocking ridge in cluster 1 bore high similarity with those in cluster 3 (Figure 5e), which likely originated from the Ural Mountains and arrived at the western Laptev at an early date. These cold air masses were wrongly classified into cluster 1. In this situation, the northwestern route originating from the Ural Mountains dominated the early 2021 event, which was consistent with the result of the air trajectory density (Figure 2b).

The northwestern and northern routes were also detected via the daily surface air temperature drop from the final day in both events in Bueh et al.'s study [2]. According to the surface air temperature drop intensity, Bueh et al. [2] further noted that the northwestern path dominated the late 2020 event, while the northern path dominated the early 2021 event. In view of the extreme cold air masses path, a larger amount of air mass moved along the northern route in the late 2020 event, but along the northwestern route in the early 2021 event in this study. Note that Bueh et al. [2] only tracked the surface air temperature drop intensity from 3 January for the early 2021 event, and pointed out that the northern route dominated. We looked further back to 1 January, and found that the cold air in the northern route on 3 January was from the Ural Mountains in the northwestern route. Thus, the northwestern route dominated the early 2021 event in this study. Most cold air masses in the two events passed through the extreme cold area (mean isotherms lower than -32°C) around Yakutsk, facilitating the extremeness of the two cold events [2]. In particular, a western path appeared when using LAGRANTO, which was different from the northwestern path in cold air source and moving path. Moreover, the cold air masses along the west path reached the northern of the Tianshan Mountains around (42°N – 47°N , 80°E – 90°E) earlier than the others in both events (Figure 5). Intriguingly, the height anomaly over the north of the Tianshan Mountains became positive when the cold air arrived on 27 December 2020 (Figure 5b) and continued until 8 January 2021. Thus, a question arises as to the role of the early arrival of the cold air over the north of the Tianshan Mountains in the successive cold events.

4. Influence of Cold Air over the North of the Tianshan Mountains in the Western Path

Figure 6 shows the daily air temperature, geopotential height, and sea level pressure anomalies averaged over (42°N – 47°N , 80°E – 90°E). Note that the climatological surface pressure of this region was 838 hPa due to the terrain; thus, we analyzed the air temperature and the corresponding height anomalies above 850 hPa. The temperature anomaly became negative on 27 December 2020 and remained so until 8 January 2021 (Figure 6a). This suggests that cold air accumulated over the north of the Tianshan Mountains from 27 December 2020. Meanwhile, the sea level pressure increased from 27 December 2020 to 8 January 2021 (Figure 6b). As a result, the positive height anomaly was amplified and its center located at a low level (\sim below 700hPa), it therefore lagged behind the negative air temperature anomaly center by one day (Figure 6a). The positive height anomaly could have caused the blocking ridge over the polar moving southward to enter China [7].

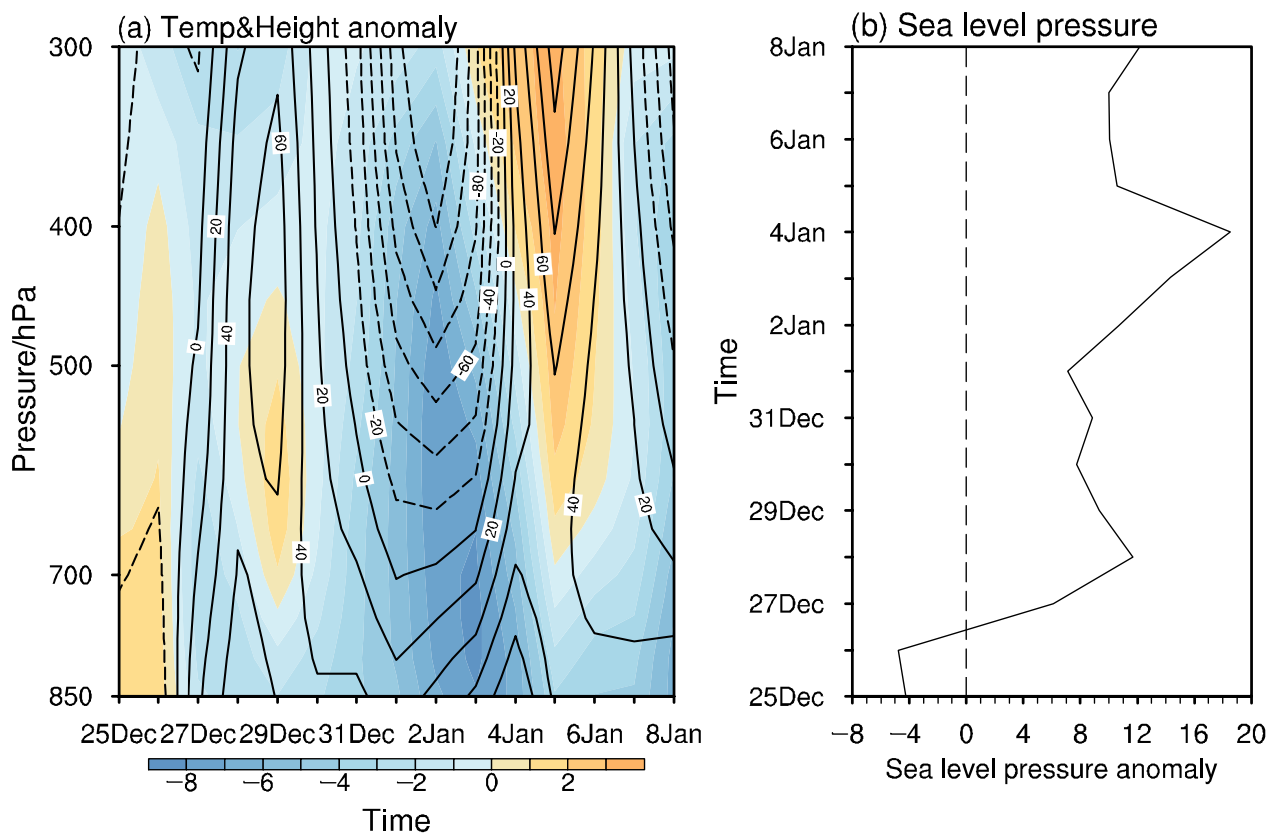


Figure 6. (a) The time–pressure cross-section of air temperature anomaly (contour, unit: °C) and geopotential height anomaly (shading, unit: gpm). (b) Daily sea level pressure anomaly (unit: hPa) averaged over (42° N–47° N, 80° E–90° E) from 25 December 2020 to 8 January 2021.

We further verified the role of the near-surface cold air on the positive height anomaly over the key region (42° N–47° N, 80° E–90° E) using piecewise PV inversion. A pressure level of 850 hPa was set as the boundary level. The height anomaly inverted from the bottom boundary condition was attributed to the response of the surface cold anomaly according to Equation (4). Figure 7 shows the daily 850 hPa geopotential height anomaly inverted from the surface cold anomalies at 850 hPa. The cold anomalies at the boundary decreased the intervals between the isentropic surface. Correspondingly, the static stability increased and led to a negative vorticity anomaly due to the conservation of PV [29,30]. Thus, the surface cold resulted in an overlying positive height anomaly. The positive height anomaly with northerlies over the southwest of Lake Baikal contributed to cold air advections from the mid-high latitude regions hitting China. From the 850 hPa height anomaly inverted from PV at each level (Figure 8a), the positive height anomaly at 850 hPa mainly resulted from the bottom boundary thermal anomaly—that is, from the surface cold air—thus highlighting the influence of surface cold.

Noteworthy, the cold air accumulated over the north of the Tianshan Mountains from the late 2020 event to the early 2021 event. The corresponding northerly anomalies over the west of Lake Baikal induced the cold air southward and devoted to the second cold event (the early 2021 event), suggesting that the active role of cold air over the north of the Tianshan Mountains on the successive cold events. Moreover, cold air disappeared and the height anomaly turned to be negative after 10 January 2021 (Figure 8b). This interrupted the cold air southward and may terminate the coming third cold event.

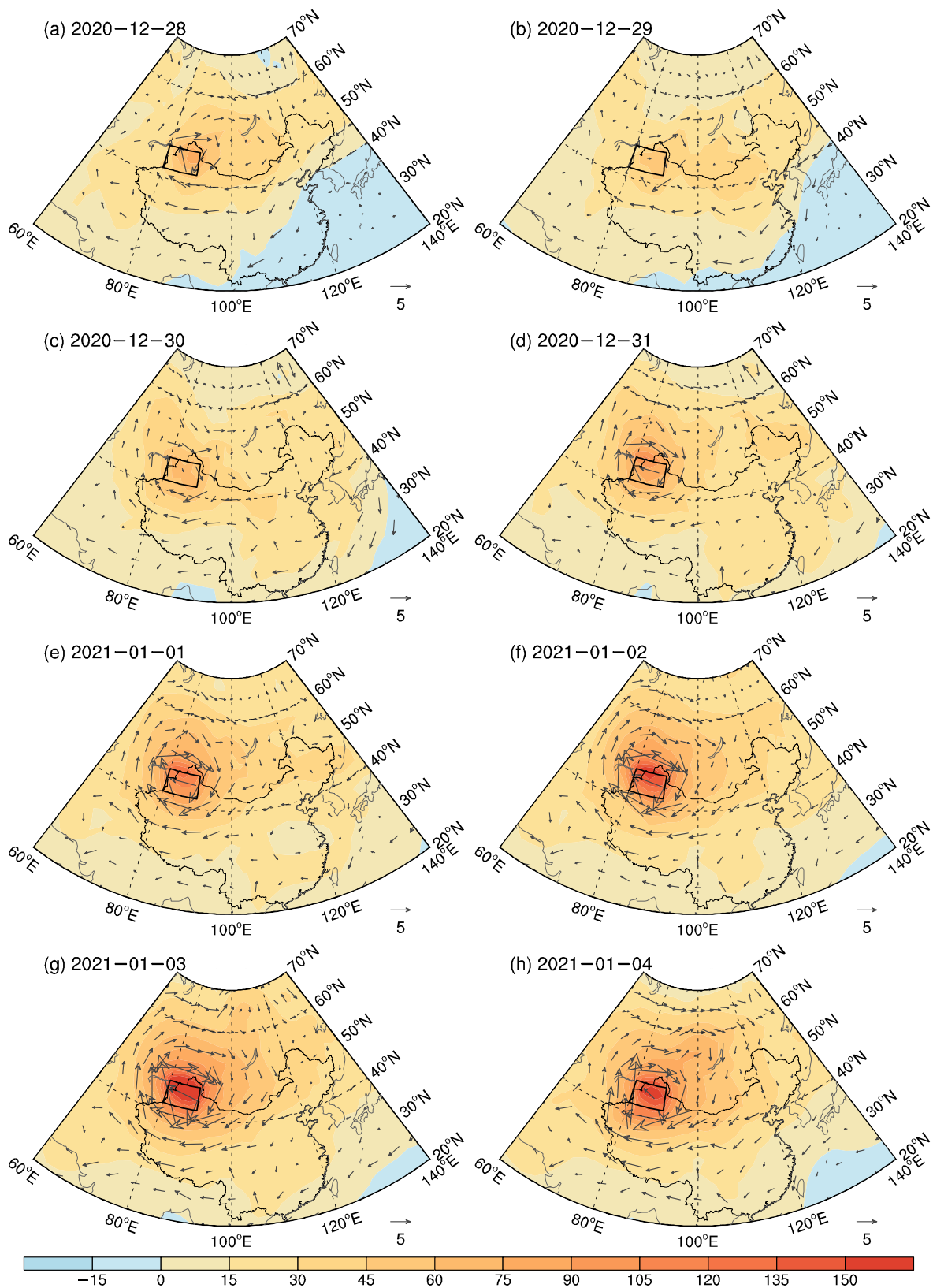


Figure 7. Daily 850 hPa geopotential height anomaly (shading, unit: gpm) and wind anomalies (arrows, units: m s^{-1}) via the piecewise PV inversion on 850 hPa (a–h) from 28 December 2020 to 4 January 2021. The black box is the key region over (42° N–47° N, 80° E–90° E).

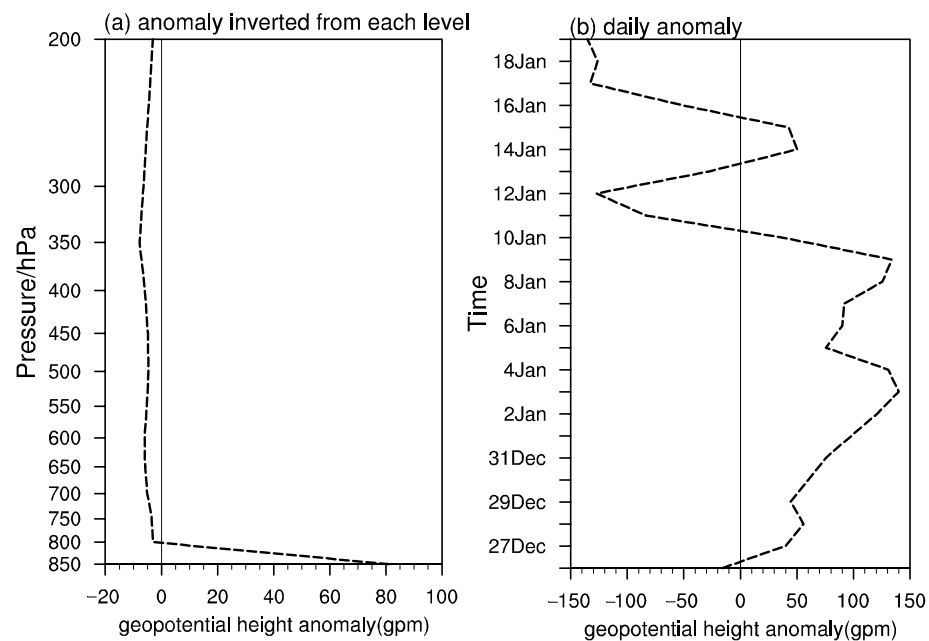


Figure 8. (a) 850 hPa geopotential height anomaly averaged over (42° N– 47° N, 80° E– 90° E) inverted from the piecewise PV inversion on each level averaged from 28 December 2020 to 4 January 2021. (b) same as (a) but for daily geopotential height anomaly inverted from the 850 hPa PV.

5. Conclusions and Discussion

5.1. Conclusions

This study aimed to isolate the cold air pathways and their key regions and to further explore their connecting role in the two successive extreme cold events in China during 28–31 December 2020 and 6–8 January 2021. Three cold air sources with three cold air routes were identified from a Lagrangian perspective. The cold air in the western route over the north of the Tianshan Mountains played a crucial role in connecting the two extreme cold events. The main conclusions are as follows:

(1) LAGRANTO tracked three cold air sources for the two events. The northern cold air source was over the eastern Laptev Sea, the northwestern source, and western source were over the west of the Ural Mountains and over the west of Lake Balkhash and the Tianshan Mountains, respectively. The northern source was relatively southward, while the northwestern and western sources were more eastward in the early 2021 event than in the late 2020 event.

(2) The *K*-means method classified three cold air routes. The northern route dominated the late 2020 event, which originated from the eastern Laptev Sea and headed southward; while the northwestern route from the Ural Mountains moving clockwise controlled the early 2021 event. The cold air along the western route, which originated from the west of Lake Balkhash and the Tianshan Mountains in the late 2020 event (the eastern Qinghai-Tibet Plateau in the early 2021 event), played a relatively small role in the two events. Moreover, according to the daily cold air locations, the cold air attacking North and East China was along the northern route, while that invading central Inner Mongolia was along the northwestern and western routes in the late 2020 event. In the early 2021 event, the cold air along the western, northern and northwestern routes hit the eastern Qinghai-Tibet Plateau, South China and North China, respectively.

(3) The cold air along the western route arrived at the north of the Tianshan Mountains earlier than the other two routes and amplified the local positive height anomaly. As the cold air accumulated, the positive height anomaly enhanced and guided the cold air from the northern and northwestern routes southward, allowing it invade China from the late 2020 event to the early 2021 event, which further caused the successiveness of the two cold events.

5.2. Discussion

Previous studies have discerned the key circulations in the troposphere and stratosphere and remote forcing in relation to these two events as such events rarely occur, especially in succession [2,4,6,9]. Moreover, the cold air itself plays a crucial role in the overlying circulation via modulating the static stability, which has not been analyzed. This study evaluated the cold air trajectory during the two events and highlighted the cold air over the north of the Tianshan Mountains which guided cold air southward in the other routes and further devoted to the continuous occurrences of the early 2021 event. However, the connecting role of cold air over the north of the Tianshan Mountains was conjectured from the successive cold events in the 2020/21 winter, but this connecting role needs more successive cases for further verification.

Author Contributions: Conceptualization and methodology, L.Z. and Z.X.; data curation and visualization, L.Z. and S.H.; writing—original draft preparation, L.Z.; writing—review and editing, Z.X. and L.Z. All authors have read and agreed to the published version of the manuscript.

Funding: This research was jointly funded by the National Natural Science Foundation of China (Grant No., 42005033 and 41875078).

Institutional Review Board Statement: Not applicable.

Informed Consent Statement: Not applicable.

Data Availability Statement: The ERA5 dataset on pressure levels is from <https://cds.climate.copernicus.eu/cdsapp#!/dataset/reanalysis-era5-pressure-levels?tab=overview> (accessed on 3 March 2022), while that on model levels for LAGRANTO is from <https://apps.ecmwf.int/data-catalogues/era5/?class=ea> (accessed on 3 March 2022).

Conflicts of Interest: The authors declare no conflict of interest.

References

1. Zhang, X.D.; Yu, Y.F.; Han, Z.; Overland, J.E.; Rinke, A.; Tang, H.; Vihma, T.; Wang, M.Y. Extreme cold events from East Asian to North America in winter 2020/21: Comparisons, Causes, and Future implications. *Adv. Atmos. Sci.* **2022**, *39*, 553–565. [CrossRef]
2. Bueh, C.; Peng, J.; Lin, D.; Chen, B. On the Two Successive Supercold Waves Straddling the End of 2020 and the Beginning of 2021. *Adv. Atmos. Sci.* **2022**, *39*, 591–608. [CrossRef]
3. Han, R.; Shi, L.; Yuan, Y. Analysis on the causes of cold and warm transition in China during the winter of 2020/2021. *Meteor. Mon.* **2021**, *47*, 880–892. (In Chinese)
4. Zheng, F.; Yuan, Y.; Ding, Y.; Li, K.; Fang, X.; Zhao, Y.; Sun, Y.; Zhu, J.; Ke, Z.; Wang, J.; et al. The 2020/21 extremely cold winter in China influenced by the synergistic effect of La Nina and Warm Arctic. *Adv. Atmos. Sci.* **2022**, *39*, 546–552. [CrossRef]
5. Dai, G.; Li, C.; Han, Z.; Luo, D.; Yao, Y. The Nature and Predictability of the East Asian Extreme Cold Events of 2020/21. *Adv. Atmos. Sci.* **2022**, *39*, 566–575. [CrossRef]
6. Yu, Y.Y.; Li, Y.F.; Ren, R.C.; Cai, M.; Guan, Z.Y.; Huang, W. An isentropic mass circulation view on the extreme cold events in 2020/21 Winter. *Adv. Atmos. Sci.* **2022**, *39*, 643–657. [CrossRef]
7. Peng, J.B.; Sun, S.Q.; Chen, B.M. Maintenance, and development of the Ural high and its contribution to severe cold wave activities in winter 2020/21. *Atmos. Ocean. Sci. Lett.* **2021**, *15*, 100130. [CrossRef]
8. Hoskins, B.J.; McIntyre, M.E.; Robertson, A.W. On the use and significance of isentropic potential vorticity maps. *Q. J. R. Meteorol. Soc.* **1985**, *111*, 877–946. [CrossRef]
9. Yao, Y.; Zhang, W.; Luo, D.; Zhong, L.; Pei, L. Seasonal cumulative effect of Ural blocking episodes on the frequent cold events in China during the early winter of 2020/21. *Adv. Atmos. Sci.* **2022**, *39*, 609–624. [CrossRef]
10. Zhang, R.N.; Screen, J.A.; Zhang, R.H. Arctic and Pacific Ocean conditions were favourable for cold extremes over Eurasia and North America during Winter 2020/21. *Bull. Am. Meteorol. Soc.* **2022**, *103*, E2285–E2301. [CrossRef]
11. Bretherton, F.P. Critical layer instability in baroclinic flows. *Q. J. R. Meteorol. Soc.* **1966**, *92*, 325–334. [CrossRef]
12. Takaya, K.; Nakaruma, H. Mechanisms of intraseasonal amplification of the cold Siberian high. *J. Atmos. Sci.* **2005**, *62*, 4423–4440. [CrossRef]
13. Xie, Z.; Black, R.X.; Deng, Y. Planetary and synoptic-scale dynamic control of extreme cold wave patterns over the United States. *Clim. Dyn.* **2019**, *53*, 1477–1495. [CrossRef]
14. Zhang, L.; Xie, Z.; Deng, Y.; Huang, W. Structure and Large-scale organization of extreme cold wave events over the Chinese mainland during the boreal cold season. *J. Geophys. Res.* **2021**, *126*, e2021JD035005. [CrossRef]

15. Xie, Z.; Bueh, C.; Zhuge, A.; Lian, R.; Liao, Z.; Yan, J.; Lin, D. An intensification of warm and moist convey belt of Asian summer monsoon in “21.7” Henan rainstorm and its key circulation from quasi-geostrophic potential vorticity perspective. *Chin. J. Atmos. Sci.* **2022**, *46*, 1147–1166. [[CrossRef](#)]
16. Ding, Y. Build-up, air mass transformation and propagation of Siberian high and its relation to cold surge in East Asia. *Meteor. Atmos. Phys.* **1990**, *44*, 281–292.
17. Papritz, L. Arctic lower-tropospheric warm and cold extremes: Horizontal and vertical transport, diabatic processes, and linkage to synoptic circulation features. *J. Clim.* **2020**, *33*, 993–1016. [[CrossRef](#)]
18. Cai, B.; Zeng, G.; Li, Z. Autumn cold surge paths over North China and the associated atmospheric circulation. *Atmosphere* **2019**, *10*, 134. [[CrossRef](#)]
19. Tao, S.Y. Studies of cold waves over East Asia in China in recent 10 years. *Acta Meteorol. Sin.* **1959**, *30*, 226–230. (In Chinese)
20. Shang, L. Cold wave knowledge. *Meteor. Mon.* **1975**, *2*, 13–15. (In Chinese)
21. Hersbach, H.; Bell, B.; Berrisford, P.; Hirahara, S.; Horanyi, A.; Muñoz-Sabater, J.; Nicolas, J.; Peubey, C.; Radu, R.; Schepers, D.; et al. The ERA5 global reanalysis. *Q. J. R. Meteorol. Soc.* **2020**, *146*, 1999–2049. [[CrossRef](#)]
22. Sprenger, M.; Wernli, H. The LAGRANTO lagrangian analysis tool-Version 2.0. *Geosci. Model. Dev.* **2015**, *8*, 2569–2586. [[CrossRef](#)]
23. Bieli, M.; Pfahl, S.; Wernli, H. ALagrantian investigation of hot and cold temperature extremes in Europe. *Q. J. R. Meteorol. Soc.* **2015**, *141*, 98–108. [[CrossRef](#)]
24. Milligan, G.W.; Cooper, M.C. An examination of procedures for determining the number of clusters in a data set. *Psychometrika* **1985**, *50*, 159–179. [[CrossRef](#)]
25. Xie, Z.; Black, R.X.; Deng, Y. Daily-scale planetary wave patterns and the modulation of cold season weather in the northern extratropics. *J. Geophys. Res. Atmos.* **2017**, *122*, 8383–8398. [[CrossRef](#)]
26. Kodinariya, T.M.; Makwana, P.R. Review on determining number of Cluster in K-Means Clustering. *Int. J. Adv. Res. Comput. Sci. Manag. Stud.* **2013**, *1*, 90–95.
27. Opiyo, S.; Okinda, C.; Zhou, J.; Mwangi, E.; Makange, N. Medial axis-based machine-vision system for orchard robot navigation. *Comput. Electron. Agric.* **2021**, *185*, 106153. [[CrossRef](#)]
28. Nielsen-Gammon, J.W.; Lefevre, R.J. Piecewise tendency diagnosis of dynamical processes governing the development of an upper-tropospheric mobile trough. *J. Atmos. Sci.* **1996**, *53*, 3120–3142. [[CrossRef](#)]
29. Shou, S.W. Theory and Application of Potential Vorticity. *Meteor. Mon.* **2010**, *36*, 9–18. (In Chinese)
30. Ding, Y.H.; Ma, X.Q. Analysis of isentropic potential vorticity for a strong cold wave in 2004/2005 winter. *Acta Meteorol. Sin.* **2007**, *65*, 695–707. (In Chinese)